RSC Advances

PAPER

View Article Online
View Journal | View Issue

Cite this: *RSC Adv.*, 2017, **7**, 2544

Fabrication of the reduced preoxidized graphene-based nanofiltration membranes with tunable porosity and good performance†

Yanhong Chang,*[ab] Yudi Shen,[abc] Debin Kong,*[c] Jing Ning,[c] Zhichang Xiao,[cd] Jiaxu Liang[cd] and Linjie Zhi*[c]

Received 5th October 2016
Accepted 1st December 2016

DOI: 10.1039/c6ra24746f

www.rsc.org/advances

A series of reduced preoxidized graphene membranes (rPGMs) were prepared by reducing the preoxidized graphene membranes (PGMs) at different reduction times. The pore morphology of the membranes and the changes in the specific porosity values along with the water flux parameters were investigated. In addition, the membranes were able to maintain a high dye rejection (>97.5% for methyl orange (MO)) and a good rejection ratio for salt ions (71.2% for $MgSO_4$). The preoxidized graphene-based nanofiltration membranes with tunable porosity exhibit great potential as high-precision molecular sieves for water purification and other applications.

In the coming decade, lack of clean water will be a formidable challenge due to the fast growth in population, persistent droughts, and an increase in demand. Among all possible approaches for tackling the water crisis, nanofiltration (NF) technology is now widely used for drinking water and waste water treatment, owing to its low energy cost and convenient operational process.[1–5]

Traditional NF membranes are manufactured from polymers or other materials, which are designed as a dense physical barrier or as a size-selective sieve.[6] Engineered graphene oxide (GO) has demonstrated a strong potential as an ultrathin, ultrafast, and yet accurate sieving membrane for aqueous ions, permitting the transport of solutes based on their ion size or differences in the ion diffusion/deposition rates.[7–10] Especially, owing to the frictionless and ultrafast water flow inside the well-defined carbon nanochannels,[11] GO membranes are thought to have significant potential in the water treatment applications.[12–18] Due to the high aspect ratio of GO sheets, these graphene membranes can be simply obtained either by vacuum filtration or spin-coating from a GO solution. The low-cost and environmentally benign fabrication process make these graphene membranes suitable for large-scale production.[19] Because of the strong hydrogen bonds and hydrophobic interactions between the GO sheets, these graphene membranes are able to retain their structural integration in water.[20–22]

Alternatively, reduced graphene oxide (rGO) nanosheets, which allow the gases and ions with relatively smaller sizes to permeate, have also recently attracted increased attention for their application in liquid and gas separation.[9,23] In addition, rGO membranes, with a layered structure similar to that of the GO films, exhibit better stability in water as they can retain the compact interlayer spacing due to the significantly reduced amount of the hydrated functional groups.[24] The main challenge for the rGO membranes in aqueous separation lies in their high resistance to transport due to their narrowed interlayer spacing. Geim *et al.*[7] found that thick rGO membranes of about 0.5–1.0 μm were impermeable to all molecules including water. However, the permeability of rGO can be improved by decreasing the thickness of the membrane. Li *et al.*[8] recently reported that when the thickness of a rGO membrane is reduced to the nanometer scale, it becomes permeable to hydrogen and water molecules, which might be due to the spanning of the channels formed by the structural defects in the rGO nanosheets across the membranes. On the other hand, Huang *et al.* recently reported that because of their highly porous structure and significantly reduced channel length, the nanostrand-channelled GO ultrafiltration membranes with a network of 3–5 nm nanochannels exhibited a superior separation performance compared to that of the unmodified GO membranes, without sacrificing the rejection rate.[25] Ultrathin graphene nanofiltration membranes for water purification based on physical sieving and electrostatic interaction mechanisms were also fabricated.[26]

[a]*Department of Environmental Engineering, University of Science and Technology of Beijing, Xueyuan Road No. 30, Haidian District, Beijing, 100083, P. R. China. E-mail: yhchang@ustb.edu.cn; Tel: +86 10 62333292*

[b]*Beijing Key Laboratory of Resource-oriented Treatment of Industrial Pollutants, University of Science and Technology of Beijing, Xueyuan Road No. 30, Haidian District, Beijing, 100083, P. R. China*

[c]*National Center for Nanoscience and Technology, Beiyitiao No. 11, Zhongguancun, Beijing, 100190, P. R. China. E-mail: zhilj@nanoctr.cn; kongdb@nanoctr.cn; Fax: +86 10 82545578; Tel: +86 10 82545578*

[d]*University of Chinese Academy of Sciences, Beijing 100039, P. R. China*

† Electronic supplementary information (ESI) available. See DOI: 10.1039/c6ra24746f

Additionally, the mass transportation in these graphene membranes (GMs) and reduced graphene membranes (rGMs) greatly relies on the microstructure and feed graphene derivatives. The nanochannel, formed by the adjacent graphene flakes or wrinkled graphene in GMs, leads to a wide range of pure water flux values.[27,28] Li *et al.* first prepared GMs by vacuum filtration using chemically converted graphene and explored their potential applications in the nanofiltration process, which showed a pure water flux of 40 L m^{-2} h^{-1} bar^{-1} and a rejection rate of 67% for Direct Yellow.[4] Mi *et al.* deposited GO on a porous support and 1,3,5-benzenetricarbonyl trichloride to show a 26% rejection for a 0.01 M Na_2SO_4 solution with a water flux of about 25 L m^{-2} h^{-1} bar^{-1}.[11] Moreover, taking an advantage of the graphene oxide intercalated with the carbon nanotubes, Han *et al.* reported that the nanofiltration membrane showed a high dye rejection and a good rejection rate for the salt ions with a water flux of 11.3 L m^{-2} h^{-1} bar^{-1}.[29]

Although previously reported GMs and rGMs showed a high pure water flux and rejection rate to some degree, ion-selective NF membranes have rarely been reported. In this study, we report a conceptually different method to fabricate the preoxidized graphene-based nanofiltration membranes with tunable porosity as molecular sieves, by introducing the in-plane carbon vacancy defects (pores) into the graphene sheets. These in-plane pores on the PGMs provide a high density of new, cross-plane diffusion channels that facilitate the infiltration of water molecules and reject the dyes or salt ions. Additionally, this method can be designed to analyze the changes in the pore dimensions and hybrids with new functionalities.

The design for the PGMs and rPGMs was based on GO. The fabrication process is outlined in Scheme 1. In-plane porosity was introduced into GO *via* a wet chemical method that combined ultrasonic vibration and a mild acid oxidation[1] (Scheme 1a). Based on the experimental conditions, the volume ratio of GO suspension and 70% HNO_3 solution was 1 : 12.5. The ultrasound at sufficient acoustic pressures creates high strain rates and frictional forces in the cavitation bubbles, which attack the carbonaceous surface and break the framework.[8–10] Then, HNO_3 reacts with the coordinatively unsaturated carbon atoms from the GO sheets. After this, the preoxidized graphene (PG) solution (Scheme 1b), with defects in the GO suspension, was coated on the commercialized microfiltration membranes (*e.g.*, polyvinylidene fluoride (PVDF) or mixed cellulose ester membranes) as supporting substrates *via* a rod coating method[30] (Scheme 1c). Before this step, a certain amount of Pd as a catalyst (weight percentage of 10%) was added into the PG suspension, forming a Pd/PG dispersion.[31] After reduction for 20 min, 40 min, 60 min, and 80 min, a series of rPGMs were obtained (Scheme 1d), as illustrated in Scheme 1.

The raw material of GO and PG was characterized by the transmission electron microscopy (TEM), as shown in Fig. 1. The exfoliated GO sheets are observable in Fig. 1a–c. After a process of differential ultrasonic oxidation, the PG sheets showed relatively varying degrees of oxidation and exhibited different pore sizes (ranging from ~5 to 10 nm) on the surface (Fig. 1d and e). The PG sheets obtained after an ultrasonic time of 9 h were selected due to their higher porosity.[32] It can also be seen that an increase in the ultrasonic time in the solution resulted in an increase in the number and size of the nanopores on the PG sheets.

The PGMs for possible nanofiltration were designed considering that a high solvent permeability requires the membrane to be as thin as possible.[7] Accordingly, our PGMs were readily prepared by rod-coating an extremely diluted PG dispersion on the commercialized microfiltration substrate, which shows a well-aligned lamellar structure and mechanical performance (Fig. 2a). PG sheets laminate together as a result of π–π conjugation in the solvent, similar to the GO sheets, as it is known.[8] The surface of the membrane was smooth and no obvious corrugation was observed.[23] To obtain the tightly stacked membranes and further investigate the porosity, PGMs were reduced for 20 min (rPGM-20), 40 min (rPGM-40), 60 min (rPGM-60), 80 min (rPGM-80), and 100 min (rPGM-100). The first image in Fig. 2b corresponds to the PGM, which is not reduced, as a blank control. The color changes from light to dark on the surface, which can be clearly observed. Moreover, the stability of the membranes are investigated by vacuum membrane distillation (Fig. S1, ESI†). The rPGMs can retain their structure even at a high salt concentration of 4 mol L^{-1}

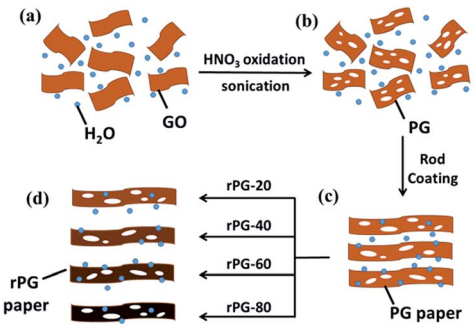

Scheme 1 Schematic for the introduction of nanopores in the preoxidized graphene (PG) papers (a–c). The reduced preoxidized graphene (rPG) papers after different times (20 min, 40 min, 60 min, and 80 min) (d).

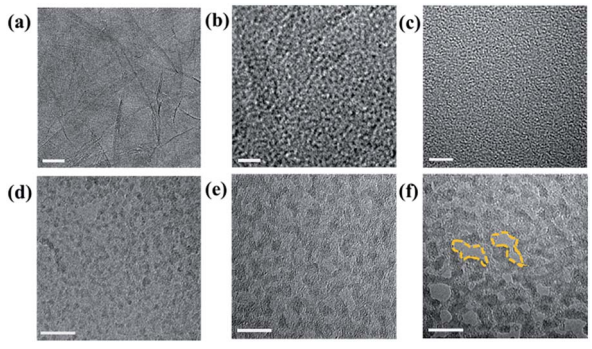

Fig. 1 TEM images of GO at different scales (a–c) and PG after various ultrasonic times: (d) 4 h, (e) 6 h, and (f) 9 h. The image shows the average pore size of the PG sheets in the ring-shaped arrangements (f). Scale bars: (a) 100 nm, (b) 10 nm, (c) 5 nm, and (d–f) 10 nm.

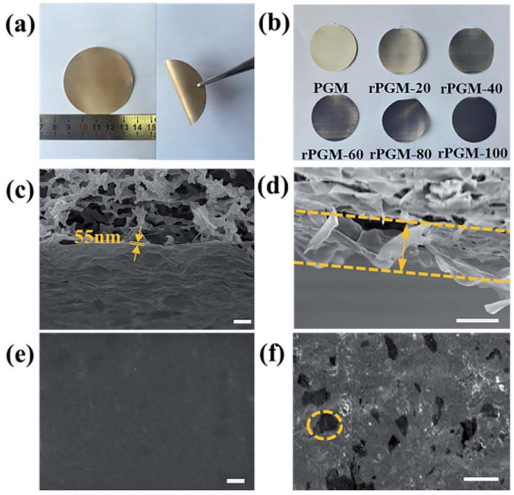

Fig. 2 (a) PG (1 mol L^{-1}) on the filter membrane (left) and the flexibility of the PGM (right). (b) Images of the rPGMs obtained at different reduction times (left to right: PGM (rPGM-0), rPGM-20, rPGM-40, rPGM-60, rPGM-80, and rPGM-100). (c and d) SEM images of the cross-section of the PGM. (e and f) The surface morphology of the rPGM-20. The ring shape indicates the average lateral length of the sheets. Scale bars: (c) 1 μm, (d) 50 nm, (e) 100 nm, and (f) 1 μm.

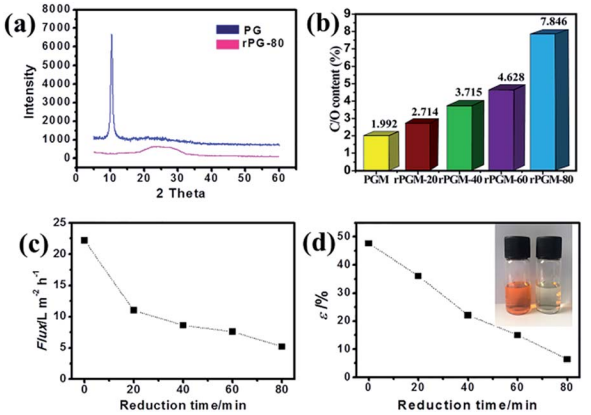

Fig. 3 (a) XRD patterns of PG and rPG-80. (b) The C/O contents as a function of their properties of the PGM and rPGM-20, rPGM-40, rPGM-60, rPGM-80. (c) Variations of pure water flux as a function of PG and rPG coated on the membranes. The pressure applied here was 1 bar. (d) The ε value of the PGM and various rPGMs at different reduction time, and after the NF process, change in the color of 0.025 g L^{-1} MO solution (left) and the collected filtrate (right) (inset).

accompanied by a pressure of 2 bar. With the purpose of investigating the mechanism through which graphene sheets stack on the supporting microporous filters, the PGM and rPGMs were characterized by scanning electron microscopy (SEM) (Fig. 2c and d). For the PGM and rPGMs, smoothness and flattening are quite important to form uniform 2D nano-channels for water transport and to achieve a high water flux. The average thickness of a PG layer was measured to be 55 nm by SEM (Fig. 2c), and Fig. 2d showed the distinct cross-section of the PG sheets. Considering the different rPGMs, reduction time did not play a significant role in the surface morphology.[23] The microstructure of rPGMs at different reduction times was obtained by SEM (Fig. 2e and f and S2, ESI†). Benefiting from the mild reaction conditions employed in this study, graphene sheets retained their structure during the reducing procedure, yielding a similar lateral length (around 0.7 μm) for all the rPGMs at different reduction times after the differential centrifugation fractionation. Additionally, with an increase in the reduction time, the zoomed SEM images of the film (Fig. 2e and S2(a), (c) and (e)†) demonstrate some wrinkles on the surface of rPGMs, indicating the appearance of a wrinkled reduced-preoxidized graphene.

The crystalline structures of the PGMs and rPGMs were characterized by X-ray diffraction (XRD) analyses. However, the average interlayer spacing between the PG and rPG sheets was required to estimate the pore size based on the X-ray diffraction.[33] One main peak at $2\theta = 10.8°$ is observed in the XRD pattern of PG in the powder state (Fig. 3a and S3, ESI†), which corresponds to an interlayer spacing of 0.82 nm.[33] Upon increasing the reduction time, the peak intensity weakens. The presence of a broad latter peak indicates that PGM has indeed been partially reduced. Note that in the spectrum of rPGM-80, only a broad peak at $2\theta = 26.8°$ was observed. Moreover, the XRD pattern for rPGM-100 is similar to that of the rPGM-80, which could probably be attributed to the complete reduction at 80 min (Fig. S3, ESI†). It implied that the PGM had already been fully reduced to rPGM and most of the oxygen-containing functional groups disappeared.[30] As a result, the XRD data can demonstrate the reduction level of PG. However, in this case, it showed limited information about the interlayer spacing of rPG. Furthermore, X-ray photoelectron spectroscopy (XPS) is commonly used for the quantitative analysis of C, O, and other elements. Fig. 3b displays the carbon to oxide ratio for PG and a series of rPG sheets. Apparently, the ratio decreased with an increase in the reduction time of the PGMs. Thus, the interlayer spacing of PGM and rPGMs (Table 1) can be obtained through a calculation according to the carbon to oxide ratio (Fig. 3b).[33]

The water transport performance of the PGM and a series of rPGMs were evaluated by measuring the water flux. These membranes were fabricated according to different reduction times, ranging from 0 to 80 min and the 100 min reduction time was excluded because a low value of water flux was obtained when the reduction time was this high (Fig. 3c). The water flux was determined until it reached a steady state. The steady-state value of the water flux could be as high as 22.2 L m^{-2} h^{-1} bar^{-1}

Table 1 Relevant parameters for PGM and rPGMs based on the Hagen–Poiseuille formula

Sample	Interlayer spacing h (nm)	Pure water flux (L m^2 h^{-1} bar^{-1})
PGM	0.82	22.2
rPGM-20	0.60	11.0
rPGM-40	0.44	8.6
rPGM-60	0.35	7.6
rPGM-80	0.21	5.3

for the non-reduced PGM. As shown in Fig. 3c, an exponential decrease in the water flux was observed for the rPGMs as the reduction time was increased. The PGM with porous channels achieved the highest water flux under a steady state (22.2 L m^{-2} h^{-1} bar^{-1}) due to its high porosity (Fig. 1f), which was a considerably high value compared to that achieved using the commercial nanofiltration membranes (for example, the pure water flux achieved with commercial membrane UTC60 is 15.4 L m^{-2} h^{-1} bar^{-1}).[1] The water flux value obtained with the PGM is also comparable to that of a recently reported ultrathin graphene nanofiltration membrane (21.8 L m^{-2} h^{-1} bar^{-1}).[26] In addition, the average water contact angle increased from 11.9° for the PGM to 121.2° for the rPGM-80 (Fig. S4, ESI†), indicating the more hydrophobic nature of rPGMs upon prolonging the reduction time, which results in a gradual decrease in the water flux value.

The Hagen–Poiseuille equation is usually employed for the theoretical estimation of the mass flow through the porous materials per unit area when the fluid behaves as a classical liquid.[34,35] Given the average size of the water nanochannels of PGM and rPGMs, under a pressure of ΔP (1 bar), the Hagen–Poiseuille equation can be transformed into the following formula (1):

$$\text{Flux} = \frac{h^4 \times \Delta P}{12L^2 \times \eta \times \Delta x} \quad (1)$$

where h is the interlayer spacing, the vertical space between the adjacent graphene sheets, which is listed in Table 1. η is the viscosity of water (0.001 Pa s at 20 °C); Δx is the thickness of the membranes, and L is the average lateral length of the graphene sheets. However, in this case, L will vary because of the different pore channels of the PGM and rPGMs. Also, for better illustration of the quantitative changes of the pore channels in the nanofiltration membranes with different reduction times, a new parameter, ε, was introduced to represent the specific porosity of the pore channels in the PGMs and rPGMs. Moreover, L can be transformed into L'/ε, where L' is the apparent average lateral length of the PG and rPG sheets (0.7 μm).[23] Thus, it was concluded that when L'/ε increased, the membrane porosity decreased, where ε is similar to a porosity parameter. Therefore, the original formula (1) can be transformed into the following formula (2):

$$\text{Flux} = \frac{h^4 \times \Delta P}{12(L'/\varepsilon)^2 \times \eta \times \Delta x} \quad (2)$$

Since water molecules might go through the defects in the PG sheets, high flux could be explained by the slip flow theory.[26] Comparing the experimental results, there may be some errors for the estimated fluxes from the modified Hagen–Poiseuille equation. Nevertheless, errors within a certain range can be ignored. Note that the graphene sheets with less oxygen-containing groups would block water molecules to a higher extent because of the strong interaction between them. Hence, only the graphene regions with functional groups were responsible for the fast transport of water.[7] Thus, based on the abovementioned data, an $\varepsilon_{PGM} = 47.6\%$ could be first obtained. Afterwards, a series of ε values could be calculated for each rPGM, those values being $\varepsilon_{rPGM\text{-}20} = 36.1\%$, $\varepsilon_{rPGM\text{-}40} = 22.1\%$, $\varepsilon_{rPGM\text{-}60} = 15.0\%$, and $\varepsilon_{rPGM\text{-}80} = 6.4\%$ (Fig. 3d). Especially, with the increase in the reduction time, the interlayer spacing between the rPG sheets became narrower and the number of pore channels in the membranes also decreased, leading to a lower specific porosity (ε) value. In addition, the trend for the ε values is basically consistent with the changes in the water flux. Thus, based on these results, the parameter ε gives the specific porosity values of the entire PG and rPG sheets obtained at different reduction times. Also, it is a facile method to evaluate the level of porosity of the membranes.

In addition, the NF performance of the PGM and rPGMs was systematically investigated. A NF membrane is a type of pressure-driven membrane with a pore size of about 0.5–2.0 nm, which can reject 90% of the material with molecular weight ranging from 200 to 1000 Da.[36] The separation ability of these NF membranes lies between those of the non-porous reverse osmosis (RO) membranes and porous UF membranes.[37,38] The pore size of the PGM and rPGMs is decided by the size of the graphene capillaries. As reported in ref. 9, the space between the graphene flakes is 1–2 nm in the hydrated state, which is within the range of that of a NF membrane. Taking advantage of the low friction for water flow inside the network of 2D nanochannels, PGMs and rPGMs were shown to have great potential in the NF applications. In our study, the rejection rate for Na_2SO_4 was up to 69.0% without any loss in the water flux (Table 2). For most of the membranes, the salt rejection rate is $R(Na_2SO_4) > R(MgSO_4) > R(NaCl) > R(MgCl_2)$, which shows a typical performance of the negatively charged NF membranes.[2] The salt rejection mechanism of the charged NF membranes is usually explained by a combination of Donnan exclusion and steric hindrance effect.[37] Note that the surface charge of the PGM and rPGMs was highly negative.[29] This agrees with the fact that the carboxyl groups on the edges of PG and rPG were retained after reflux in water.[39,40] According to the Donnan exclusion theory, as water molecules diffuse through the membrane, driven by the applied pressure, the negative charges on the PGM and rPGMs will repel the anions away from the membrane and at the same time cations will also be retained because of the electroneutrality requirements. This mechanism will result in a high rejection for the salts with multivalent anions and monovalent cations.[41] Thus, the membranes are predicted to have the highest rejection rate for

Table 2 Nanofiltration performances of PGM and rPGMs at different reduction times

	Salts (R%)				Dyes (R%)
Sample	Na_2SO_4	NaCl	$MgSO_4$	$MgCl_2$	MO
PGM	31.2	25.5	16.1	7.6	91.0
rPGM-20	46.2	44.3	24.9	8.7	95.1
rPGM-40	58.7	37.6	38.6	16.5	96.4
rPGM-60	55.3	46.9	52.1	15.0	96.9
rPGM-80	69.0	53.9	71.2	28.1	97.5

Na_2SO_4 and the lowest for $MgCl_2$, which coincides with the results displayed in Table 2. However, rPGM-80 showed a higher rejection for $MgSO_4$ than that for Na_2SO_4 because the hydrated radius value of Mg^{2+} (0.43 nm) is larger than that of Na^+ (0.36 nm), indicating that in some cases, the steric hindrance effect played a key role in the salt removing ability.[2] In addition, a rejection rate approaching 70% for Na_2SO_4 can be ascribed to a structure with densely and uniformly packed graphene sheets.[11,25,42] The reason for this is that the Donnan exclusion effect is the dominant factor for rPGM-80 while filtrating Na_2SO_4, and at high concentrations, electrolytes screen the negative charge on the graphene sheets, which weakens the Donnan exclusion effect.[43] For all PGM and rPGM, the Donnan exclusion effect was also evaluated under high ionic strength; however, the steric hindrance effect also played an important role. Moreover, for the organic dye removal tests, PGM and rPGMs exhibited an excellent dye rejection ability (Table 2). The negatively charged MO was selected as the target molecule to test the dye removal ability of PGM and rPGMs. MO was selected because its molecular weight is 327, which is very close to the lower limitations of the NF process. Almost all the membranes showed a very high rejection rate for MO (>90%). Particularly, rPGM-80 showed the highest rejection rate of 97.5% for MO (the color change of MO is displayed in the Fig. 3d inset), which indicated less paths for the MO permeation. As a result, the rejection rate of rPGM-80 for MO was the highest than that for the other rPGMs obtained with shorter reduction times. For comparison, some previously reported comparable results for the GO-based membranes applied to salt and dye removal are summarized in Table S1 (ESI†). As shown in the table, the rPGM-80 membrane in our study provides competitive results among the GO-based membranes, especially for Na^+ and dye removal. All the abovementioned results demonstrate that PG is able to retain the space between the graphene layers and maintain a high water flux.

Using PG and rPG, novel NF membranes with high water flux and high rejection rate for salt and dyes can be obtained. The method not only provides a new design idea for adjusting the pore size of the graphene membranes, but also gives a new insight for exploring the water transport between the graphene layers. Hence, further research for better integration of the mechanism of the abovementioned results with film applications is needed in the future studies.

In summary, PGM and rPGMs were fabricated for investigating the change in the porosity along with the water flux parameters. The rPG sheets with sub-10 nm sized compactly stacked 2D nanocapillaries and the hydrophobic carbon nanochannels presented an advantage for the high water flux. According to the Hagen–Poiseuille equation, a new parameter ε was introduced and a series of specific porosity values for PGM and rPGMs were obtained. According to the value of ε, the changes in the porosity on the membranes can be quantitatively analyzed. Furthermore, upon testing the NF performance, it was concluded that the rPGM can maintain a high dye rejection rate for MO (>90%) and also a high ion rejection rate. The study exploring the 2D pore channels from the point of water flux provides a facile approach to fabricate the porous materials for the environment, energy, and other applications. In addition, a further enhanced performance of the PGMs and rPGMs, including an optimized pore size and pore density on the sheets, has a promising potential for desalination, removal of heavy metals, and other fields.

Acknowledgements

The authors gratefully acknowledge the financial supports from the National Natural Science Foundation of China (Grant no. 21276023, 21476025, 20973044, 21173057, 21273054, 51425302 and 51302045), the Ministry of Science and Technology of China (no. 2012CB933400 and 2012CB933403), the Beijing Municipal Science and Technology Commission (Z121100006812003), the Chinese Academy of Sciences, and the China Scholarship Council.

Notes and references

1 K. O. Agenson, J.-I. Oh and T. Urase, *J. Membr. Sci.*, 2003, **225**, 91–103.
2 J. Schaep, B. Van der Bruggen, C. Vandecasteele and D. Wilms, *Sep. Purif. Technol.*, 1998, **14**, 155–162.
3 K. Kimura, G. Amy, J. E. Drewes, T. Heberer, T.-U. Kim and Y. Watanabe, *J. Membr. Sci.*, 2003, **227**, 113–121.
4 D. Li, M. B. Muller, S. Gilje, R. B. Kaner and G. G. Wallace, *Nat. Nanotechnol.*, 2008, **3**, 101–105.
5 S. J. Gao, H. Qin, P. Liu and J. Jin, *J. Mater. Chem. A*, 2015, **3**, 6649–6654.
6 S. R. Lewis, S. Datta, M. Gui, E. L. Coker, F. E. Huggins, S. Daunert, L. Bachas and D. Bhattacharyya, *Proc. Natl. Acad. Sci. U. S. A.*, 2011, **108**, 8577–8582.
7 R. R. Nair, H. A. Wu, P. N. Jayaram, I. V. Grigorieva and A. K. Geim, *Science*, 2012, **335**, 442–444.
8 H. Li, Z. Song, X. Zhang, Y. Huang, S. Li, Y. Mao, H. J. Ploehn, Y. Bao and M. Yu, *Science*, 2013, **342**, 95–98.
9 R. K. Joshi, P. Carbone, F. C. Wang, V. G. Kravets, Y. Su, I. V. Grigorieva, H. A. Wu, A. K. Geim and R. R. Nair, *Science*, 2014, **343**, 752–754.
10 K. Celebi, J. Buchheim, R. M. Wyss, A. Droudian, P. Gasser, I. Shorubalko, J.-I. Kye, C. Lee and H. G. Park, *Science*, 2014, **344**, 289–292.
11 M. Hu and B. Mi, *Environ. Sci. Technol.*, 2013, **47**, 3715–3723.
12 H. W. Kim, H. W. Yoon, S.-M. Yoon, B. M. Yoo, B. K. Ahn, Y. H. Cho, H. J. Shin, H. Yang, U. Paik, S. Kwon, J.-Y. Choi and H. B. Park, *Science*, 2013, **342**, 91–95.
13 N. Wei, X. Peng and Z. Xu, *ACS Appl. Mater. Interfaces*, 2014, **6**, 5877–5883.
14 D. W. Boukhvalov, M. I. Katsnelson and Y.-W. Son, *Nano Lett.*, 2013, **13**, 3930–3935.
15 S. K. Kannam, B. D. Todd, J. S. Hansen and P. J. Daivis, *J. Chem. Phys.*, 2012, **136**, 024705.
16 D. Cohen-Tanugi and J. C. Grossman, *Nano Lett.*, 2012, **12**, 3602–3608.
17 S. C. O'Hern, M. S. H. Boutilier, J.-C. Idrobo, Y. Song, J. Kong, T. Laoui, M. Atieh and R. Karnik, *Nano Lett.*, 2014, **14**, 1234–1241.

18 C.-N. Yeh, K. Raidongia, J. Shao, Q.-H. Yang and J. Huang, *Nat. Chem.*, 2015, **7**, 166–170.
19 D. A. Dikin, S. Stankovich, E. J. Zimney, R. D. Piner, G. H. B. Dommett, G. Evmenenko, S. T. Nguyen and R. S. Ruoff, *Nature*, 2007, **448**, 457–460.
20 P. Sun, M. Zhu, K. Wang, M. Zhong, J. Wei, D. Wu, Z. Xu and H. Zhu, *ACS Nano*, 2013, **7**, 428–437.
21 Z. Xu and C. Gao, *Acc. Chem. Res.*, 2014, **47**, 1267–1276.
22 L. Peng, Z. Xu, Z. Liu, Y. Wei, H. Sun, Z. Li, X. Zhao and C. Gao, *Nat. Commun.*, 2015, **6**, DOI: 10.1038/ncomms6716.
23 H. Liu, H. Wang and X. Zhang, *Adv. Mater.*, 2015, **27**, 249–254.
24 B. Mi, *Science*, 2014, **343**, 740–742.
25 H. Huang, Z. Song, N. Wei, L. Shi, Y. Mao, Y. Ying, L. Sun, Z. Xu and X. Peng, *Nat. Commun.*, 2013, **4**, DOI: 10.1038/ncomms3979.
26 Y. Han, Z. Xu and C. Gao, *Adv. Funct. Mater.*, 2013, **23**, 3693–3700.
27 L. Qiu, X. Zhang, W. Yang, Y. Wang, G. P. Simon and D. Li, *Chem. Commun.*, 2011, **47**, 5810–5812.
28 Y. P. Tang, D. R. Paul and T. S. Chung, *J. Membr. Sci.*, 2014, **458**, 199–208.
29 Y. Han, Y. Jiang and C. Gao, *ACS Appl. Mater. Interfaces*, 2015, **7**, 8147–8155.
30 J. Ning, J. Wang, X. Li, T. Qiu, B. Luo, L. Hao, M. Liang, B. Wang and L. Zhi, *J. Mater. Chem. A*, 2014, **2**, 10969.
31 M. Liang, J. Wang, B. Luo, T. Qiu and L. Zhi, *Small*, 2012, **8**, 1180–1184.
32 X. Wang, L. Jiao, K. Sheng, C. Li, L. Dai and G. Shi, *Sci. Rep.*, 2013, **3**, 1996.
33 A. Akbari, P. Sheath, S. T. Martin, D. B. Shinde, M. Shaibani, P. C. Banerjee, R. Tkacz, D. Bhattacharyya and M. Majumder, *Nat. Commun.*, 2016, **7**, 10891.
34 M. Majumder, N. Chopra and B. J. Hinds, *ACS Nano*, 2011, **5**, 3867–3877.
35 J. K. Holt, H. G. Park, Y. Wang, M. Stadermann, A. B. Artyukhin, C. P. Grigoropoulos, A. Noy and O. Bakajin, *Science*, 2006, **312**, 1034–1037.
36 S. P. Sun, T. A. Hatton, S. Y. Chan and T.-S. Chung, *J. Membr. Sci.*, 2012, **401–402**, 152–162.
37 N. Hilal, H. Al-Zoubi, N. A. Darwish, A. W. Mohamma and M. Abu Arabi, *Desalination*, 2004, **170**, 281–308.
38 W. R. Bowen and J. S. Welfoot, *Chem. Eng. Sci.*, 2002, **57**, 1121–1137.
39 D. R. Dreyer, S. Park, C. W. Bielawski and R. S. Ruoff, *Chem. Soc. Rev.*, 2010, **39**, 228–240.
40 K. Erickson, R. Erni, Z. Lee, N. Alem, W. Gannett and A. Zettl, *Adv. Mater.*, 2010, **22**, 4467–4472.
41 J. M. M. Peeters, J. P. Boom, M. H. V. Mulder and H. Strathmann, *J. Membr. Sci.*, 1998, **145**, 199–209.
42 H. Huang, Y. Mao, Y. Ying, Y. Liu, L. Sun and X. Peng, *Chem. Commun.*, 2013, **49**, 5963–5965.
43 X.-L. Wang, T. Tsuru, S.-i. Nakao and S. Kimura, *J. Membr. Sci.*, 1997, **135**, 19–32.